Environmental Science & Technology

Article

pubs.acs.org/est

# Impact of Sunlight and Humic Acid on the Deposition Kinetics of Aqueous Fullerene Nanoparticles ($nC_{60}$)

Xiaolei Qu, Pedro J.J. Alvarez, and Qilin Li*

Department of Civil and Environmental Engineering, Rice University, Houston, Texas 77005, United States

Supporting Information

**ABSTRACT:** Nanoparticle transport in natural settings is complex due to interactions with the surrounding environment. In this study, the impact of UVA irradiation and humic acid (HA) on deposition of aqueous fullerene nanoparticles ($nC_{60}$) on a silica surface as a surrogate for natural sediments was studied using packed column experiments and quartz crystal microbalance with dissipation monitoring under various solution conditions. Surface oxidation of $nC_{60}$ induced by UVA irradiation greatly retarded its deposition due to the increased negative surface charge and hydrophilicity. Dissolved HA, once adsorbed onto the $nC_{60}$ surface, also hindered its deposition mainly through steric hindrance forces. The extent of this effect depended on the properties and the amount of HA adsorbed, which is a function of ionic strength and HA concentration. HA has limited adsorption on UVA-irradiated $nC_{60}$ and is expected to play a less important role in its stability. HA immobilized onto the silica surface had a variable effect on $nC_{60}$ deposition, depending on the complex interplay of Derjaguin–Landau–Verwey–Overbeek (DLVO) and non-DLVO interactions such as electrostatic interaction, steric hindrance, and hydrogen bonding as well as HA molecular conformation. These results highlight the importance of environment-induced changes in $nC_{60}$ surface chemistry in its fate and transport in aquatic environments.

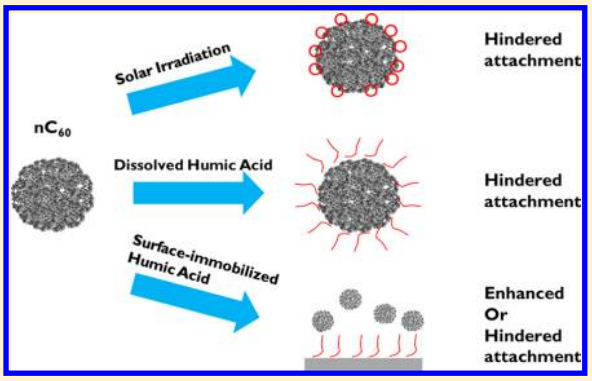


## INTRODUCTION

Buckminsterfullerene ($C_{60}$) has drawn much attention due to its unique physicochemical properties such as antioxidative properties, photoactivity, hydrophobicity, the spherical cage structure, and high electron affinity, which could enable a wide range of potential applications including optics, cosmetics, and pharmaceuticals.[1] The current and potential use in consumer products and large-scale production of $C_{60}$ will inevitably lead to its release into the environment. Modeling studies predicted the concentrations of fullerenes at the order of magnitude of nanograms per liter to micrograms per liter in surface waters and micrograms per liter in wastewater treatment plant effluents.[2] Because $C_{60}$ as a molecule has extremely low solubility in water ($1.3 \times 10^{-8}$ ng/L ~ 7.96 ng/L),[3,4] the nanosized colloidal particle of $C_{60}$ formed in the aqueous phase, usually referred to as $nC_{60}$, is considered a more environmentally relevant form of fullerene. Many studies showed that $nC_{60}$ can exert toxicity to various organisms such as bacteria, fish, and human cell lines,[5−7] raising concerns regarding its potential impact to human and ecosystem health. Initial studies postulated that reactive oxygen species (ROS) generation is one of the major toxicity mechanisms involved.[8,9] However, reports on the ROS generation of $nC_{60}$ were contradictory. Several studies reported minimal to no ROS production by aqueous $nC_{60}$ due to self-quenching.[10,11] Thus, it has been suggested that the toxicity of $nC_{60}$ stems from ROS-independent oxidative stress.[12,13]

Unlike conventional contaminants such as dissolved organic compounds and heavy metals, the fate and transport of nanoparticles are largely controlled by aggregation and deposition processes.[14] A number of studies have investigated the transport of $nC_{60}$ in model porous media as well as natural soils using packed column experiments or quartz crystal microbalance with dissipation monitoring (QCM-D).[15−24] These studies suggest that the properties of $nC_{60}$ and the collectors, solution chemistry, and hydrodynamic conditions are the major factors governing the deposition process. The deposition of $nC_{60}$ is qualitatively in good agreement with the classic DLVO theory and mostly happens in the primary minimum.[19] However, the majority of past studies were carried out with pristine $nC_{60}$ in simple electrolyte solutions. Once released into the environment, $nC_{60}$ will interact with various environmental components, including sunlight and natural organic matter (NOM), which could alter its surface chemistry and consequently confound its environmental behavior.

Ubiquitous in aquatic systems and soil, natural organic matter is a known key determinant of colloid transport. Dissolved humic acid has been shown to readily adsorb on $nC_{60}$ and enhance $nC_{60}$ colloidal stability in water.[25,26] On the other

Received: July 18, 2012
Revised: November 5, 2012
Accepted: November 16, 2012

   dx.doi.org/10.1021/es3029044 | Environ. Sci. Technol. XXXX, XXX, XXX−XXX

hand, the effect of surface-immobilized macromolecules (e.g., humic acid in organic-rich soil/sediment) on $nC_{60}$ deposition has been found to vary. Humic acid and alginate were found to retard $nC_{60}$ deposition through steric repulsion,[16] while an extracellular polymeric substance (EPS) enhanced the deposition of $nC_{60}$.[23]

Recent studies suggest that solar irradiation induced photochemical transformation could be an important fate process of $nC_{60}$ in aquatic environments.[27−30] Hou and Jafvert reported surface oxidation and decomposition of $nC_{60}$ during long-term solar irradiation.[27,28] Hwang and Li showed that $nC_{60}$ underwent surface oxidation under irradiation of UVA light, the major UV component in sunlight.[30] The oxygen-containing functional groups formed during UVA irradiation greatly hindered the aggregation of $nC_{60}$ in NaCl solutions due to the increased negative surface charge and hydrophilicity.[26] On the other hand, $Ca^{2+}$ can interact with the functional groups and destabilize UVA-irradiated $nC_{60}$. However, the effect of solar irradiation on the deposition pattern of $nC_{60}$ has not been addressed in the literature.

In the present study, deposition of $nC_{60}$ under environmentally relevant conditions was investigated by introducing UVA irradiation and humic acid, in either dissolved or surface-immobilized form, into the experimental system. The main objective was to determine the role of $nC_{60}$ surface transformation (surface oxidation under sunlight and addition of humic acid) in its deposition behavior. $nC_{60}$ irradiated by UVA for varying periods of time was thoroughly characterized, and its deposition kinetics on bare and humic acid coated silica surfaces measured under different solution conditions was compared to that of pristine $nC_{60}$. $nC_{60}$ deposition kinetics was directly measured by QCM-D and compared to that determined by conventional packed column experiments. To our knowledge, this is the first study addressing the effect of solar irradiation on $nC_{60}$ deposition. Along with our earlier paper regarding the impact of sunlight and humic acid on $nC_{60}$ aggregation,[26] findings from this study underscore the important role of solar irradiation in the environmental fate and transport of $nC_{60}$, suggesting that a better quantitative understanding of environment-induced changes in $nC_{60}$ surface chemistry is crucial to predicting its environmental transport and fate.

## MATERIALS AND METHODS

**Materials.** Sublimed $C_{60}$ powder (>99%) was purchased from Materials Electronics Research Corporation (Tucson, AZ). Suwannee River humic acid standard (II) (SRHA) and Elliott Soil humic acid (EHA) were purchased from the International Humic Substances Society (Atlanta, GA). Humic acid (HA) stock solutions were prepared by stirring the HA solutions in the dark for 24 h followed by filtration through 0.45 $\mu$m pore size nylon membrane filters (Whatman, Piscataway, NJ). The concentrations of HA stock solutions were determined using a high-sensitivity total organic carbon (TOC) analyzer (Shimadzu Scientific Instruments, Columbia, MD) based on the carbon content of SRHA (52.6%) and EHA (58.1%).[31] Poly-L-lysine (PLL, P-1274), reagent-grade NaCl, and two types of pure silica sands, with particle size 0.5−10 $\mu$m (silica sand 1) and 5−15 nm (silica sand 2) were obtained from Sigma−Aldrich (St. Louis, MO). 4-(2-Hydroxyethyl)-1-piperazineethanesulfonic acid (HEPES) was purchased from Fisher Scientific (Pittsburgh, PA). All solutions were prepared with ultrapure water generated by an E-pure system (Barnstead, Dubuque, IA).

**Preparation of $nC_{60}$ Stock Suspension.** The aqueous $nC_{60}$ stock suspension was prepared using a direct sonication protocol. A total of 150 mg of pulverized $C_{60}$ powder was mixed with 200 mL of deionized water in a 500 mL glass beaker and sonicated at 100 W with a sonicating probe (Vibra-Cell VCX 500, Sonics & Material, Newtown, CT) for 30 min in an ice bath. The resulting mixture was filtered through 2 $\mu$m pore size Millex-AP membrane filters (Millipore, Billerica, MA) to remove large particles. All filters were washed with 10 mL of ultrapure water before use and replaced after 30 mL of filtrate was collected. The concentration of the resulting $C_{60}$ suspension was 11 mg/L as measured by TOC. It was diluted to 10 mg/L and stored in the dark at room temperature. The intensity based mean hydrodynamic diameter of $nC_{60}$ was determined by dynamic light scattering (DLS, Zen 3600 zetasizer Nano, Malvern, Worcestershire, UK) to be 162 ± 5 nm. All experiments were performed within 5 months, during which the stock suspension was stable as confirmed by monitoring the particle size distribution.

**UVA Irradiation Experiments.** Since UVA is the main component of UV light in the solar spectrum, a light source in UVA wavelength was used to simulate the UV portion in solar irradiation. In the irradiation experiments, aliquots of 30 mL of $nC_{60}$ stock suspension were added to 50 mL Erlenmeyer flasks and sealed with parafilm with vents. In each experiment, four flasks were placed on the merry-go-round at the center of a Luzchem LZC-4 V photoreactor (Luzchem, Ottawa, Ontario, Canada). Four 8 W black lamps (Hitachi FL8BL-B, $\lambda$ = 350 ± 50 nm), two on each side, provided a total irradiation intensity of 2 mW/cm$^2$ in the middle of the reactor as measured by a radiometer at 350 nm (Control Company, Firendwoods, TX). Ambient air was circulated through the photoreactor, and the temperature was maintained at 25 ± 3 °C. Samples were withdrawn on the 20th hour and 7th day and stored in the dark at room temperature before analysis. The surface oxygen content of $nC_{60}$ with different irradiation time was determined by X-ray photoelectron spectroscopy (XPS, PHI Quanteria, Chanhassen, MN). To prepare samples for XPS analysis, 50 mL of sample suspension was filtered through a 0.1 $\mu$m membrane filter (Millipore, Billerica, MA) to collect $nC_{60}$ on the membrane surface. The solid cake was dried in a vacuum oven at −85 kPa and 100 °C for two days.

**$nC_{60}$ Aggregation Kinetics and Electrophoretic Mobility.** Particle size determines the diffusive mass transfer rate of colloidal particles to a surface and hence the deposition rate. $nC_{60}$ particle size during the deposition measurement was determined from aggregation kinetics measurements in the same solution chemistry (see the Supporting Information for details). The electrophoretic mobility of $nC_{60}$ and silica sands was measured in folded capillary cells (Malvern, Worcestershire, UK) by phase analysis light scattering (PALS) at 25 °C with at least five measurements per sample.

**Deposition Kinetics of $nC_{60}$.** The deposition kinetics of $nC_{60}$ on bare and humic acid (SRHA or EHA) coated silica surfaces was first studied using a QCM-D system (Q-Sense E4, BiolinScientific, Västra Frölunda, Sweden). The system is equipped with four measurement chambers each housing a 5 MHz silica-coated quartz crystal sensor (Batch 10384, Biolin Scientific, Västra Frölunda, Sweden). Before use, the silica-coated crystals were soaked in 2% SDS cleaning solution for 12 h and sonicated for 20 min. They were then copiously rinsed


dx.doi.org/10.1021/es3029044 | Environ. Sci. Technol. XXXX, XXX, XXX−XXX

with ultrapure water, dried with ultra high-purity $N_2$, and cleaned in an ozone/UV chamber (Bioforce Nanoscience, Inc., Ames, IA) for 30 min immediately prior to use. All the measurements were performed at a constant temperature of 25 °C and a flow rate of 0.1 mL/min, resulting in a laminar flow in the measurement chamber with a Reynolds number ($Re$) of 0.2. In each experiment, the electrolyte solution was first pumped through the measurement chamber until a stable baseline is achieved (i.e., the frequency signal drifts less than 1.8 Hz/h). For experiments involving dissolved humic acid, the background solution containing the electrolyte and humic acid was then introduced into the system for 20 min. Except for EHA in 100 mM NaCl, there was no humic acid adsorption on the silica surface at ionic strength up to 100 mM as reflected by the unchanged frequency. Predetermined amounts of NaCl, humic acid, and $nC_{60}$ stock solutions were mixed to form test solutions with 5 mg/L $nC_{60}$ in the solution chemistry of interest and an unadjusted pH of 6.0 ± 0.5. The resulting suspension was immediately pumped into the measurement chamber, allowing $nC_{60}$ to deposit on the silica-coated crystal surface. As the deposition took place, the increasing mass of $nC_{60}$ on the silica crystal surface hindered the vibration of the crystal and subsequently reduced the frequency. A viscoelastic deposited layer also dampened the sensor vibration, leading to energy dissipation.

The mass of a thin and rigid deposited layer on the silica crystal surface is related to the change of the frequency as described by the Sauerbrey equation:[32,33]

$$\Delta m = -\frac{C\Delta f_n}{n} \quad (1)$$

where $\Delta m$ is the deposited mass, $\Delta f_n$ is the change of frequency at overtone $n$, and $C$ is the crystal constant (17.7 ng/(Hz cm$^2$)).

For a viscoelastic layer, the Voigt model is usually used to obtain the thickness or mass and viscoelastic properties of the layer.[33] In our study, significant dissipation accompanied frequency decrease during $nC_{60}$ deposition (see representative data in the Supporting Information, Figure S1), suggesting a viscoelastic $nC_{60}$ layer. Both the frequency and the dissipation changed linearly with time during the initial deposition of $nC_{60}$, indicating continuous deposition on the clean crystal surface (i.e., no ripening or detachment). The Voigt model was employed to simultaneously fit the frequency and dissipation data at the 3rd, 5th, 7th, 9th, and 11th overtone to obtain a $nC_{60}$ deposition rate in terms of mass per unit time. The model calculated mass deposition rate correlated well with the initial slope of the frequency data (Supporting Information, Table S1 and Figure S2). Considering the limitations of the mass deposition rate calculation, for example, it assumes a homogeneous, uniform layer, and the mass calculated includes that of water in the layer, we chose to quantify the $nC_{60}$ deposition rate using the initial (200 s) slope of the frequency shift obtained at the third overtone $\Delta f_3$, which is the most stable. In order to gain insight on the physicochemical interactions between $nC_{60}$ and the surface, $nC_{60}$ deposition rates were normalized by that measured under favorable deposition conditions to obtain the attachment efficiency $\alpha$:

$$\alpha = \frac{d\Delta f_3/dt}{(d\Delta f_3/dt)_{fav}} \quad (2)$$

where $d\Delta f_3/dt$ and $(d\Delta f_3/dt)_{fav}$ are the initial slope of frequency shift measured at the third overtone in the solution of interest and that under favorable deposition conditions, respectively. In this study, the favorable deposition conditions were achieved by coating the silica crystal sensor with positively charged PLL.

Deposition of pristine $nC_{60}$ on bare sand was also examined using conventional packed column experiments to compare with the QCM-D results (see the Supporting Information for details on column experiments).

**Precoating the Silica Surface with PLL and Humic Acid.** To coat the silica crystal surface with PLL, the bare silica surface was first rinsed with a HEPES solution (10 mM HEPES, 100 mM NaCl). Then, the PLL coating solution (100 mg/L PLL, 10 mM HEPES, 100 mM NaCl) was introduced for 15 min, during which PLL adsorption reached equilibrium as suggested by the stabilized frequency. To study the deposition of $nC_{60}$ on a humic acid coated silica surface, a layer of humic acid was adsorbed on the PLL layer by flowing 10 mM NaCl followed by 10 mg/L humic acid in 10 mM NaCl for 40 min across the crystal surface. Finally, the PLL or humic acid coated surface was rinsed with the electrolyte solution used in the deposition measurement. Silica sand was used as a surrogate for the silica crystals to dertermine their surface potential. Humic acid coated silica sand was made by successively dispersing the sand in 100 mg/L PLL and 10 mg/L EHA solutions. The sand was separated from each solution by centrifugation (1000$g$ for 5 min) and thoroughly washed with ultrapure water.

## RESULTS AND DISCUSSION

**$nC_{60}$ Deposition under Favorable Conditions.** The favorable deposition rate of $nC_{60}$ as a function of NaCl concentration is presented in Figure 1. For each type of $nC_{60}$, the favorable deposition rate was constant at low ionic strength but decreased sharply as ionic strength increased. According to the aggregation data (Supporting Information, Table S2), when the $nC_{60}$ suspension entered the QCM-D measurement chamber (5 min after the $nC_{60}$ stock suspension was mixed with the NaCl solution), $nC_{60}$ nanoparticles were stable at low ionic strength (up to 10 and 150 mM for the pristine $nC_{60}$ and the 7 day UVA-irradiated $nC_{60}$ (7DUV $nC_{60}$), respectively) but aggregated at higher ionic strength. Peclet number ($Pe$), which represents the ratio of convective to diffusive mass transport, ranged from 5.9 × 10$^{-7}$ to 5.0 × 10$^{-5}$ in these deposition experiments, suggesting diffusive mass transport (see the

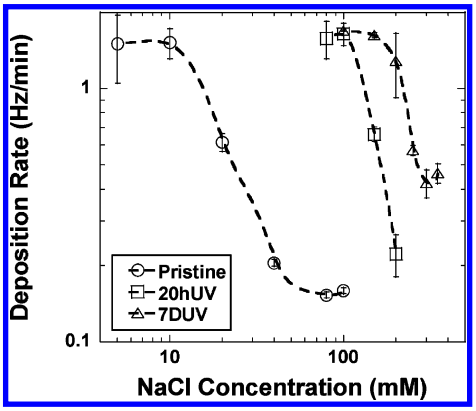


**Figure 1.** Deposition rates of pristine, 20 h UVA-irradiated (20hUV) and 7 day UVA-irradiated (7DUV) $nC_{60}$ to PLL-coated silica crystal surface (favorable deposition condition) as a function of NaCl concentration. Error bars represent standard deviation.


dx.doi.org/10.1021/es3029044 | Environ. Sci. Technol. XXXX, XXX, XXX−XXX

Supporting Information for *Pe* calculation). Therefore, the sharp decline of favorable deposition rate at higher ionic strength was attributed to the increase of particle size due to aggregation and the consequent decrease in diffusion coefficient as suggested by the Stokes−Einstein equation. Because the UVA irradiation did not change the initial particle size,[26] the favorable deposition rates of all three $nC_{60}$ were identical at low ionic strength that did not cause significant aggregation. The favorable deposition rate reached a plateau beyond a certain NaCl concentration. We hypothesize it is caused by the diffusion-limited $nC_{60}$ aggregation at NaCl concentrations beyond the critical coagulation concentration (CCC), where the aggregation rate is independent of NaCl concentration.

**Effect of UVA Irradiation.** Figure 2 compares the deposition rate and attachment efficiency of pristine and

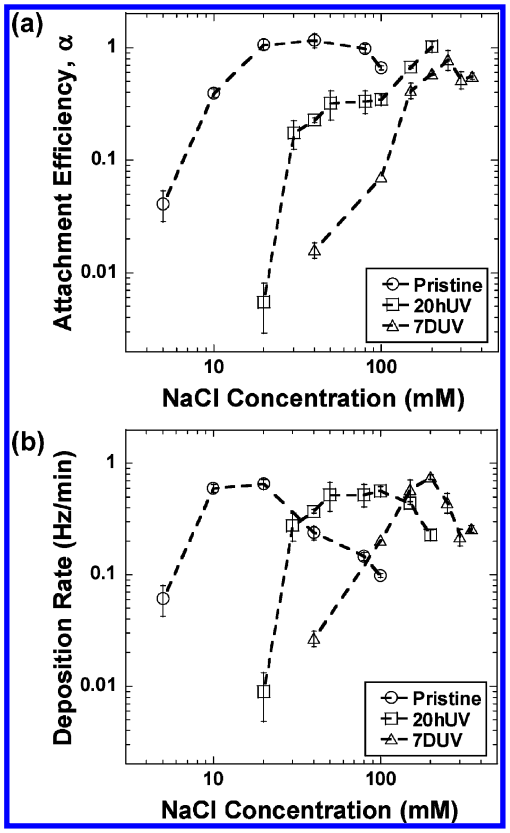


**Figure 2.** (a) Attachment efficiencies of pristine, 20hUV and 7DUV $nC_{60}$ on a silica surface as a function of NaCl concentration. Error bars represent standard deviation. (b) Deposition rates of pristine, 20hUV and 7DUV $nC_{60}$ on a silica surface as a function of NaCl concentration.

UVA-irradiated $nC_{60}$. Previous studies suggest the stability of pristine $nC_{60}$ heavily depends on the synthesis protocol and resulting nanoparticle properties, especially particle size and surface charge.[16,22,34] Nevertheless, deposition of pristine $nC_{60}$ is generally susceptible to changes in ionic strength, with a critical deposition concentration of 18 mM NaCl (Figure 2a) in this work, lower than that previously reported for $nC_{60}$ prepared by solvent exchange, 30 and 32 mM NaCl.[16,35] The deposition rate of each $nC_{60}$ was found to decrease at high ionic strength due to the decline of the mass transfer rate caused by concurrent aggregation of the nanoparticles (Figure 2b).

Figure 2a clearly shows that UVA irradiation remarkably enhanced the stability of $nC_{60}$ against deposition, consistent with our previous finding showing that UVA irradiation enhanced the stability of $nC_{60}$ against aggregation in NaCl solutions.[26] The increased stability was mainly attributed to the surface oxidation and the resulting increase in negative surface potential and hydrophilicity. XPS analysis revealed a notable increase of mono-oxygenated carbon (C—O) and dioxygenated carbon (C═O or O—C—O) on an UVA-irradiated $nC_{60}$ surface (Supporting Information, Figure S5), suggesting the introduction of oxygen-containing functional groups. The surface oxygen content of $nC_{60}$ increased with increasing UVA irradiation time from 9.3 ± 0.3% at the pristine state to 11.3 ± 0.6% after 20 h and 14.2 ± 0.6% after 7 days of irradiation (Figure 3a). As a result, the negative surface charge

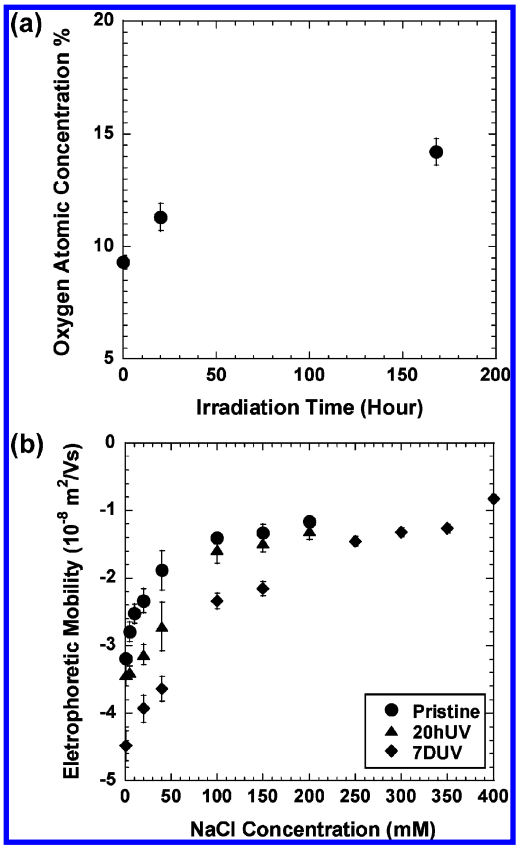


**Figure 3.** (a) Surface oxygen atomic concentration of $nC_{60}$ as a function of UVA irradiation time as measured by XPS. Error bars represent standard deviation. (b) Electrophoretic mobility of pristine, 20hUV and 7DUV $nC_{60}$ as a function of NaCl concentration.

increased with increasing irradiation time as indicated by the measured electrophoretic mobility (Figure 3b), consistent with their higher stability shown in Figure 2a. The 7DUV $nC_{60}$ was also more negatively charged than previously reported,[26] suggesting batch to batch variations of the irradiated samples. The stability of $nC_{60}$ exhibits a systematic dependence on its surface oxygen content; the sample with higher surface oxygen content tends to be more stable. A similar relationship has been reported between the colloidal stability of multiwalled carbon nanotubes and its surface oxygen concentration.[36,37]

In Figure 2a, the attachment efficiency $\alpha$ of the 7DUV $nC_{60}$ reached a maximum at 250 mM NaCl, yet its value, 0.78 ± 0.15, was notably smaller than 1. This was followed by a decrease in $\alpha$ (0.52 ± 0.09) when NaCl concentration further increased to 300 mM. However, calculation of the DLVO interaction energy


dx.doi.org/10.1021/es3029044 | *Environ. Sci. Technol.* XXXX, XXX, XXX−XXX

between the 7DUV $nC_{60}$ and the bare silica surface shows that the energy barrier disappears at 250 mM NaCl (Supporting Information, Table S3 and Figure S6). Such a discrepancy suggests that the surface oxygen functional groups can stabilize $nC_{60}$ through non-DLVO forces. Lower than unity $\alpha$ values were also observed with UVA-irradiated $nC_{60}$ in our previous study on $nC_{60}$ aggregation.[26] The decrease in attachment efficiency at high ionic strength has been reported in the deposition of bacteriophage MS2, noroviruses GI and GII, and polystyrene latex colloids on silica and glass surfaces.[38−40] These results cannot be explained by the DLVO theory[41,42] and were attributed to structural forces, likely the hydration force. The hydration force also seems to affect the deposition behavior of the pristine and 20 h UVA-irradiated (20hUV) $nC_{60}$. The attachment efficiency of both was lower than expected at NaCl concentration between 80 and 100 mM. However, the hydration force was less significant for the pristine and 20hUV $nC_{60}$ than the 7DUV $nC_{60}$ because (1) UVA irradiation increased the surface hydrophilicity of $nC_{60}$ and consequently enhanced the hydration force and (2) the hydration force is more pronounced at high ionic strength, where the surface hydrated counterions are more abundant.

The deposition kinetics of pristine $nC_{60}$ was also characterized by packed column experiments. The seepage velocity was adjusted to match the flow velocity used in the QCM-D measurements ($2 \times 10^{-4}$ m/s). The *Pe* values in the packed column and QCM-D systems are $9.6 \times 10^{-6}$ and $5.9 \times 10^{-7}$, respectively, over the ionic strength range compared, suggesting diffusive transport in both systems (see the Supporting Information for details). Representative $nC_{60}$ breakthrough curves are presented in Figure S4 of the Supporting Information. The calculated $\alpha$ values are compared to those determined by QCM-D in Figure 4. The attachment

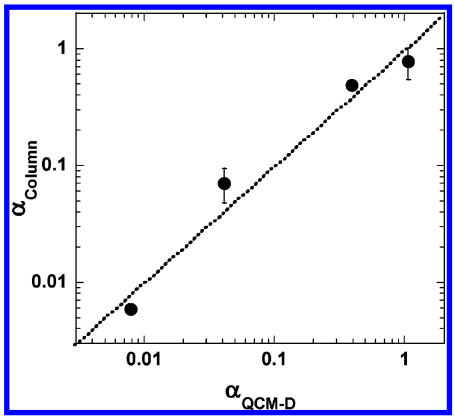


**Figure 4.** Correlation between attachment efficiencies of pristine $nC_{60}$ deposition in the packed column system and QCM-D system at the same ionic strength. Error bars represent standard deviation. Dashed line indicates the perfect consistency.

efficiency determined from the two systems, $\alpha_{column}$ and $\alpha_{QCM-D}$, agree with each other well, suggesting the relevance and applicability of QCM-D as an alternative for packed column experiments to study $nC_{60}$ deposition behavior. The QCM-D method is less time-consuming and labor intensive; it also avoids heterogeneity in porous media grain size, porosity, and surface chemistry, which contribute to discrepancies between different works.

**Effect of Dissolved Humic Acid.** As a major component of NOM, humic acid can readily adsorb onto colloidal particles via hydrophobic interactions, alter their surface physicochemical properties, and consequently change their transport pattern. Various studies have reported that dissolved humic acid could retard deposition of various colloidal particles such as $nC_{60}$, latex particles, carbon nanotubes, hematite, and titanium dioxide,[16,43−47] mainly through the steric hindrance effect. Our previous study revealed that humic acid adsorbed on $nC_{60}$ significantly enhanced the stability of $nC_{60}$ against aggregation; with 1 mg/L SRHA, the CCC of the pristine $nC_{60}$ rose from 84 to 331 mM NaCl,[26] and there was no detectable change in particle size at 100 mM NaCl (the highest ionic strength used in deposition experiments with dissolved humic acid) for at least 5 min. Because the $nC_{60}$ used in this work was prepared in the same way as our previous study, the particle size is assumed to remain unchanged in the presence of humic acid (at 1 and 5 mg/L) over the NaCl concentrations tested (5−100 mM).[26] Thus, the favorable deposition rate measured in 5 mM NaCl solution in the absence of humic acid was used for the whole ionic strength range tested.

Adsorption of dissolved humic acid can affect $nC_{60}$ deposition in two ways: (1) it hinders aggregation and hence enhances diffusive mass transfer; (2) it reduces the deposition attachment efficiency. As shown in Figure 5a, the deposition attachment efficiency was reduced by up to 1 order of magnitude in the presence of humic acid. The reduced deposition can be attributed to the change of $nC_{60}$ surface potential and the steric repulsion from adsorbed humic acid. Adsorption experiments (see the Supporting Information for

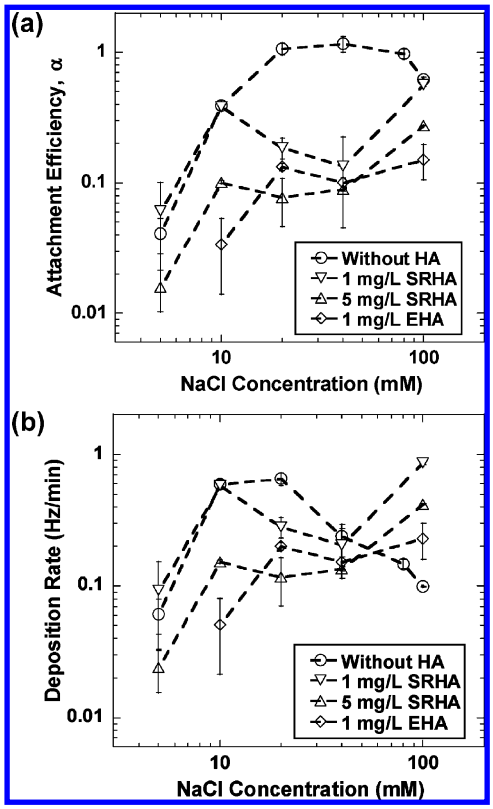


**Figure 5.** (a) Attachment efficiencies of pristine $nC_{60}$ onto a silica surface as a function of NaCl concentration in the presence of dissolved SRHA or EHA. Error bars represent standard deviation. (b) Deposition rates of pristine $nC_{60}$ onto a silica surface as a function of NaCl concentration in the presence of dissolved Suwannee River humic acid or Elliott Soil humic acid.


dx.doi.org/10.1021/es3029044 | *Environ. Sci. Technol.* XXXX, XXX, XXX−XXX

details) show that EHA and SRHA had similar adsorption on pristine $nC_{60}$ at 1 mg/L ($K_d$ = 1648 and 1722 (mg/kg)/(mg/L), respectively, Table S4 of the Supporting Information). However, EHA was more efficient than SRHA in stabilizing pristine $nC_{60}$, likely due to its higher molecular weight,[31,48,49] which results in stronger steric repulsion. In the absence of humic acid, the $nC_{60}$ attachment efficiency increased with increasing ionic strength as predicted by the DLVO theory, except for a drop at very high ionic strength as discussed earlier. In the presence of humic acid, however, the $nC_{60}$ attachment efficiency exhibited a complex, nonmonotonous behavior. Such complex behavior is a result of the interplay between the conflicting effects of ionic strength on humic acid adsorption by $nC_{60}$ and $nC_{60}$ surface potential. When ionic strength increases, the electrostatic repulsion between $nC_{60}$ and the silica surface decreases, leading to more deposition; on the other hand, the electrostatic repulsion between humic acid molecules and the $nC_{60}$ surface also decreases, resulting in more humic acid adsorption and hence greater steric hindrance effect. The effect of ionic strength on the overall $nC_{60}$ deposition efficiency is therefore the net effect of these two mechanisms. This interpretation is supported by measurement of SRHA adsorption on the pristine $nC_{60}$-coated silica surface using QCM-D (see details in the Supporting Information). At a SRHA concentration of 5 mg/L, the amount of SRHA adsorbed on the $nC_{60}$-coated silica crystal surface was 0.50 mg/m$^2$ at 10 mM NaCl and increased to 0.78 mg/m$^2$ at 40 mM NaCl. As expected, the $nC_{60}$ attachment efficiency decreased with increasing SRHA concentration due to more SRHA adsorption. The complex behavior of $nC_{60}$ attachment efficiency in the presence of humic acid clearly demonstrates that quantification of NOM adsorption is crucial to accurate prediction of $nC_{60}$ deposition. Both SRHA and EHA had negligible adsorption on the 7DUV $nC_{60}$ surface at 1 mg/L due to increased $nC_{60}$ surface hydrophilicity and negative charge after irradiation (Supporting Information, Table S4). Thus, dissolved humic acid is expected to affect the deposition of UVA-irradiated $nC_{60}$ to a much lesser extent.

The overall impact of dissolved humic acid on $nC_{60}$ deposition is the net effect of enhanced $nC_{60}$ mass transfer to the surface because of the smaller particle size and the reduced attachment efficiency (Figure 5b). The $nC_{60}$ deposition rate in the absence of humic acid initially increased with ionic strength due to the increase in attachment efficiency but declined at ionic strength greater than 20 mM due to $nC_{60}$ aggregation and hence decreased mass transfer. Dissolved humic acid reduced $nC_{60}$ deposition at low ionic strength, suggesting that the reduction in attachment efficiency due to steric hindrance outcompetes the enhanced mass transfer rate resulting from smaller particle sizes. At high ionic strength (e.g., 100 mM NaCl), however, the opposite occurred: $nC_{60}$ deposition rate in the presence of humic acid was much higher than that in the absence of humic acid, although the attachment efficiency of $nC_{60}$ is lower in the presence of humic acid (Figure 5a). This is attributed to the enhanced mass transfer rate of $nC_{60}$ in the presence of humic acid due to the smaller particle size. However, these results should not be simply interpreted as dissolved humic acid would enhance the deposition of $nC_{60}$ at high ionic strength, as $nC_{60}$ would undergo fast aggregation without humic acid and large $nC_{60}$ aggregates can be easily removed by straining in porous media, which is not reflected by the QCM-D measurement.

**Effect of Surface-Immobilized Humic Acid.** By using two pure silica sands (silica sands 1 and 2) as surrogates to the silica crystal surface, surface-immobilized humic acid was found to lower the negative surface potential of the silica crystal. As shown in Figure 6a, although the $\zeta$ potential of the two bare silica sands was drastically different, EHA-coated silica sands were similarly charged, suggesting that the surface potential of silica sands was dominated by the immobilized EHA macromolecules. The $\zeta$ potential of the bare silica crystal surface is −53 mV as measured by a SurPASS electrokinetic analyzer in 1 mM ionic strength, which is close to silica sand 1, −52 ± 2.2

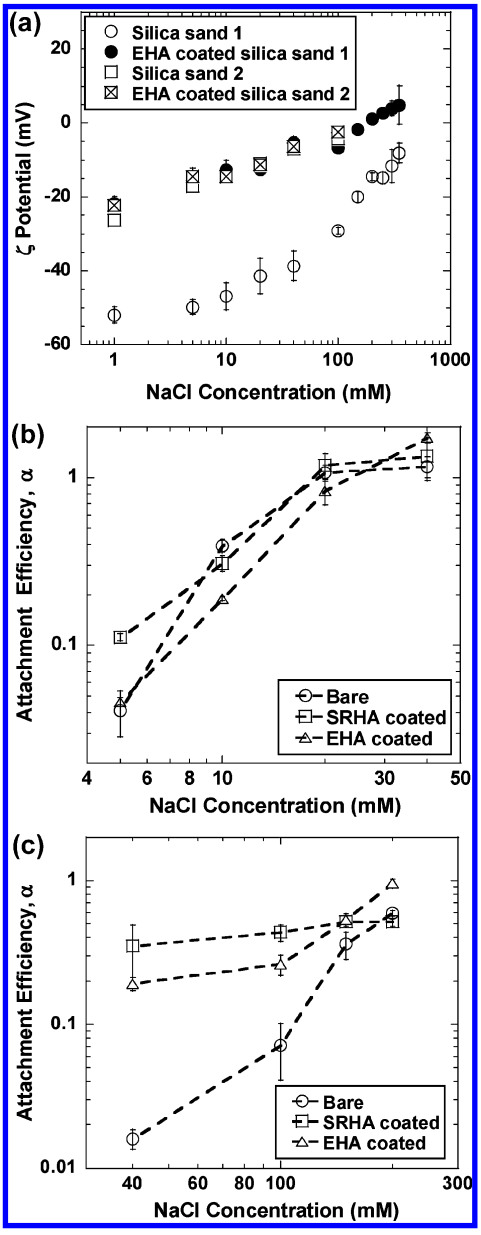


**Figure 6.** (a) $\zeta$ potentials of bare and EHA-coated silica sand as a function of NaCl concentration. Error bars represent standard deviation. The particle sizes of silica sands 1 and 2 are 0.5−10 $\mu$m and 5−15 nm, respectively. (b) Attachment efficiencies of pristine $nC_{60}$ onto bare and humic acid coated silica surfaces as a function of NaCl concentration. Error bars represent standard deviation. (c) Attachment efficiencies of 7DUV $nC_{60}$ onto bare and humic acid coated silica surfaces as a function of NaCl concentration.


dx.doi.org/10.1021/es3029044 | Environ. Sci. Technol. XXXX, XXX, XXX−XXX

mV. Therefore, an EHA-coated silica crystal surface was assumed to have the same $\zeta$ potential as EHA-coated silica sand 1. This finding qualitatively agreed with an earlier study using crushed quartz sand as a surrogate for the silica crystal.[50]

The deposition of pristine $nC_{60}$ on the EHA-coated silica surface was lower than that on the bare silica surface (Figure 6b), whereas the deposition of pristine $nC_{60}$ on the SRHA-coated silica surface was similar to that on the bare silica surface except at 5 mM. This contradicts the DLVO calculation that shows notably lower energy barrier on the EHA-coated silica surface (Supporting Information, Table S3). The reduced deposition is attributed to steric hindrance by the immobilized humic acid. This effect is more pronounced at low ionic strength because humic acid molecules have a more stretched-out conformation due to the electrostatic repulsion between charged groups.

The presence of both surface-immobilized EHA and SRHA greatly facilitated the deposition of 7DUV $nC_{60}$, and the attachment efficiency on the humic acid coated surface was less sensitive to the change of ionic strength as shown in Figure 6c. Several studies have reported enhanced colloid deposition by surface-immobilized macromolecules, including $nC_{60}$ deposition on alginate[16] and an EPS-coated silica surface,[23] and *Pseudomonas aeruginosa* deposition on an alginate-coated silica surface[51] in monovalent electrolyte solutions, which was attributed to the hydrophobic effect or physical trapping in the macromolecules. However, neither of the mechanisms applied in this case. The 7DUV $nC_{60}$ is more hydrophilic than the pristine $nC_{60}$ as a result of surface oxidation; physical trapping, if any, is expected to also enhance the deposition of the pristine $nC_{60}$, contradictory to our findings. Moreover, the effect of physical trapping will be largely suppressed at high ionic strength as the structure of humic acid becomes more compact. We hypothesize that three mechanisms are responsible for the enhanced attachment efficiency of the 7DUV $nC_{60}$ on humic acid coated silica surfaces: the diminished steric hindrance, the reduced collector surface potential, and hydrogen bonding. It has been shown that the structure and properties of immobilized macromolecules strongly depend on ionic strength.[38,52] At high ionic strength (~60 mM), the steric hindrance diminishes as the conformation of humic acid become more compact.[38,51] Thus, at the ionic strength we employed for measuring the 7DUV $nC_{60}$ deposition kinetics, 40−200 mM, the steric hindrance force was likely not prominent. DLVO calculation suggests the presence of surface-immobilized humic acid reduces electrostatic repulsion, which partially offsets the effect of steric hindrance forces and gradually became the dominant effect with increasing ionic strength. This is consistent with our observation of both pristine and 7DUV $nC_{60}$ deposition.

However, the deposition of the 7DUV $nC_{60}$ on humic acid coated silica surfaces is relatively insensitive to ionic strength, suggesting the reduced electrostatic repulsion is not the sole mechanism for the enhanced deposition. Another likely mechanism involved is hydrogen bonding between the oxygen-containing groups on the 7DUV $nC_{60}$ surface and the oxygen- and nitrogen-containing groups on surface-immobilized humic acid.

## ■ ASSOCIATED CONTENT

### Supporting Information

Details of (1) QCM-D characterization of particle deposition kinetics, (2) determination of particle size during the deposition experiments, (3) packed column experiments, (4) XPS spectra of the pristine and 7DUV $nC_{60}$, (5) DLVO interaction energy calculation, and (6) humic acid adsorption experiments. This material is available free of charge via the Internet at http://pubs.acs.org.

## ■ AUTHOR INFORMATION

### Corresponding Author

*Phone: (713) 348-2046; fax: (713) 348-5268; e-mail: qilin.li@rice.edu.

### Notes

The authors declare no competing financial interest.

## ■ ACKNOWLEDGMENTS

This work was supported by the USEPA STAR program (grant no. 834093). We thank Dr. Xin (Cissy) Ma for providing the $\zeta$ potential measurement of the bare silica crystal surface.

## ■ REFERENCES

(1) Nakamura, E.; Isobe, H. Functionalized fullerenes in water. The first 10 years of their chemistry, biology, and nanoscience. *Acc. Chem. Res.* **2003**, *36* (11), 807−815.

(2) Aschberger, K.; Micheletti, C.; Sokull-Kluttgen, B.; Christensen, F. M. Analysis of currently available data for characterising the risk of engineered nanomaterials to the environment and human health—lessons learned from four case studies. *Environ. Int.* **2011**, *37* (6), 1143−56.

(3) Heymann, D. Solubility of fullerenes $C_{60}$ and $C_{70}$ in seven normal alcohols and their deduced solubility in water. *Fullerene Sci. Technol.* **1996**, *4* (3), 509−515.

(4) Jafvert, C. T.; Kulkarni, P. P. Buckminsterfullerene's ($C_{60}$) octanol−water partition coefficient ($K_{ow}$) and aqueous solubility. *Environ. Sci. Technol.* **2008**, *42* (16), 5945−5950.

(5) Fang, J. S.; Lyon, D. Y.; Wiesner, M. R.; Dong, J. P.; Alvarez, P. J. J. Effect of a fullerene water suspension on bacterial phospholipids and membrane phase behavior. *Environ. Sci. Technol.* **2007**, *41* (7), 2636−2642.

(6) Zhu, S. Q.; Oberdorster, E.; Haasch, M. L. Toxicity of an engineered nanoparticle (fullerene, $C_{60}$) in two aquatic species, *Daphnia* and fathead minnow. *Mar. Environ. Res.* **2006**, *62*, S5−S9.

(7) Sayes, C. M.; Fortner, J. D.; Guo, W.; Lyon, D.; Boyd, A. M.; Ausman, K. D.; Tao, Y. J.; Sitharaman, B.; Wilson, L. J.; Hughes, J. B.; West, J. L.; Colvin, V. L. The differential cytotoxicity of water-soluble fullerenes. *Nano Lett.* **2004**, *4* (10), 1881−1887.

(8) Markovic, Z.; Todorovic-Markovic, B.; Kleut, D.; Nikolic, N.; Vranjes-Djuric, S.; Misirkic, M.; Vucicevic, L.; Janjetovic, K.; Isakovic, A.; Harhaji, L.; Babic-Stojic, B.; Dramicanin, M.; Trajkovic, V. The mechanism of cell-damaging reactive oxygen generation by colloidal fullerenes. *Biomaterials* **2007**, *28* (36), 5437−5448.

(9) Sayes, C. M.; Gobin, A. M.; Ausman, K. D.; Mendez, J.; West, J. L.; Colvin, V. L. Nano-$C_{60}$ cytotoxicity is due to lipid peroxidation. *Biomaterials* **2005**, *26* (36), 7587−7595.

(10) Lee, J.; Yamakoshi, Y.; Hughes, J. B.; Kim, J. H. Mechanism of $C_{60}$ photoreactivity in water: fate of triplet state and radical anion and production of reactive oxygen species. *Environ. Sci. Technol.* **2008**, *42* (9), 3459−3464.

(11) Lee, J.; Fortner, J. D.; Hughes, J. B.; Kim, J. H. Photochemical production of reactive oxygen species by $C_{60}$ in the aqueous phase during UV irradiation. *Environ. Sci. Technol.* **2007**, *41* (7), 2529−2535.

(12) Lyon, D. Y.; Brunet, L.; Hinkal, G. W.; Wiesner, M. R.; Alvarez, P. J. J. Antibacterial activity of fullerene water suspensions ($nC_{60}$) is not due to ROS-mediated damage. *Nano Lett.* **2008**, *8* (5), 1539−1543.

(13) Lyon, D. Y.; Alvarez, P. J. J. Fullerene water suspension ($nC_{60}$) exerts antibacterial effects via ROS-independent protein oxidation. *Environ. Sci. Technol.* **2008**, *42* (21), 8127−8132.

(14) Qu, X. L.; Li, Q. L.; Alvarez, P. J. J.; Choi, Y. C.; Conlon, W. J.; Diaz, I. *Review of Nanomaterial Research and Relevance for Water Reuse; WateReuse Research Foundation*, in press.
(15) Brant, J.; Lecoanet, H.; Wiesner, M. R. Aggregation and deposition characteristics of fullerene nanoparticles in aqueous systems. *J. Nanopart. Res.* **2005**, *7* (4−5), 545−553.
(16) Chen, K. L.; Elimelech, M. Interaction of fullerene ($C_{60}$) nanoparticles with humic acid and alginate coated silica surfaces: measurements, mechanisms, and environmental implications. *Environ. Sci. Technol.* **2008**, *42* (20), 7607−7614.
(17) Espinasse, B.; Hotze, E. M.; Wiesner, M. R. Transport and retention of colloidal aggregates of $C_{60}$ in porous media: effects of organic macromolecules, ionic composition, and preparation method. *Environ. Sci. Technol.* **2007**, *41* (21), 7396−7402.
(18) Wang, Y. G.; Li, Y. S.; Fortner, J. D.; Hughes, J. B.; Abriola, L. M.; Pennell, K. D. Transport and retention of nanoscale $C_{60}$ aggregates in water-saturated porous media. *Environ. Sci. Technol.* **2008**, *42* (10), 3588−3594.
(19) Wang, Y. G.; Li, Y. S.; Pennell, K. D. Influence of electrolyte species and concentration on the aggregation and transport of fullerene nanoparticles in quartz sands. *Environ. Toxicol. Chem.* **2008**, *27* (9), 1860−1867.
(20) Wang, Y. G.; Li, Y. S.; Kim, H.; Walker, S. L.; Abriola, L. M.; Pennell, K. D. Transport and retention of fullerene nanoparticles in natural soils. *J. Environ. Qual.* **2010**, *39* (6), 1925−1933.
(21) Li, Y. S.; Wang, Y. G.; Pennell, K. D.; Abriola, L. M. Investigation of the transport and deposition of fullerene (C60) nanoparticles in quartz sands under varying flow conditions. *Environ. Sci. Technol.* **2008**, *42* (19), 7174−7180.
(22) Isaacson, C.; Zhang, W.; Powell, T.; Ma, X.; Bouchard, D. Temporal changes in Aqu/$C_{60}$ physical-chemical, deposition, and transport characteristics in aqueous systems. *Environ. Sci. Technol.* **2011**, *45* (12), 5170−5177.
(23) Tong, M. P.; Ding, J. L.; Shen, Y.; Zhu, P. T. Influence of biofilm on the transport of fullerene ($C_{60}$) nanoparticles in porous media. *Water Res.* **2010**, *44* (4), 1094−1103.
(24) Chae, S. R.; Xiao, Y.; Lin, S.; Noeiaghaei, T.; Kim, J. O.; Wiesner, M. R. Effects of humic acid and electrolytes on photocatalytic reactivity and transport of carbon nanoparticle aggregates in water. *Water Res.* **2012**, *46* (13), 4053−4062.
(25) Chen, K. L.; Elimelech, M. Influence of humic acid on the aggregation kinetics of fullerene ($C_{60}$) nanoparticles in monovalent and divalent electrolyte solutions. *J. Colloid Interface Sci.* **2007**, *309* (1), 126−134.
(26) Qu, X. L.; Hwang, Y. S.; Alvarez, P. J. J.; Bouchard, D.; Li, Q. L. UV irradiation and humic acid mediate aggregation of aqueous fullerene ($nC_{60}$) nanoparticles. *Environ. Sci. Technol.* **2010**, *44* (20), 7821−7826.
(27) Hou, W. C.; Jafvert, C. T. Photochemical transformation of aqueous $C_{60}$ clusters in sunlight. *Environ. Sci. Technol.* **2009**, *43* (2), 362−367.
(28) Hou, W. C.; Jafvert, C. T. Photochemistry of aqueous $C_{60}$ clusters: evidence of $^1O_2$ formation and its role in mediating $C_{60}$ phototransformation. *Environ. Sci. Technol.* **2009**, *43* (14), 5257−5262.
(29) Li, Q. L.; Xie, B.; Hwang, Y. S.; Xu, Y. J. Kinetics of $C_{60}$ fullerene dispersion in water enhanced by natural organic matter and sunlight. *Environ. Sci. Technol.* **2009**, *43* (10), 3574−3579.
(30) Hwang, Y. S.; Li, Q. L. Characterizing photochemical transformation of aqueous $nC_{60}$ under environmentally relevant conditions. *Environ. Sci. Technol.* **2010**, *44* (8), 3008−3013.
(31) IHSS website. http://www.ihss.gatech.edu/ (accessed September 21, 2011).
(32) Sauerbrey, G. Verwendung von schwingquarzen zur wägung dünner schichten und zur mikrowägung. *Z. Phys.* **1959**, *155* (2), 206−222.
(33) Reviakine, I.; Johannsmann, D.; Richter, R. P. Hearing what you cannot see and visualizing what you hear: interpreting quartz crystal microbalance data from solvated interfaces. *Anal. Chem.* **2011**, *83* (23), 8838−8848.
(34) Chen, K. L.; Elimelech, M. Relating colloidal stability of fullerene ($C_{60}$) nanoparticles to nanoparticle charge and electrokinetic properties. *Environ. Sci. Technol.* **2009**, *43* (19), 7270−7276.
(35) Chen, K. L.; Elimelech, M. Aggregation and deposition kinetics of fullerene ($C_{60}$) nanoparticles. *Langmuir* **2006**, *22* (26), 10994−11001.
(36) Smith, B.; Wepasnick, K.; Schrote, K. E.; Bertele, A. H.; Ball, W. P.; O'Melia, C.; Fairbrother, D. H. Colloidal properties of aqueous suspensions of acid-treated, multi-walled carbon nanotubes. *Environ. Sci. Technol.* **2009**, *43* (3), 819−825.
(37) Smith, B.; Wepasnick, K.; Schrote, K. E.; Cho, H. H.; Ball, W. P.; Fairbrother, D. H. Influence of surface oxides on the colloidal stability of multi-walled carbon nanotubes: a structure−property relationship. *Langmuir* **2009**, *25* (17), 9767−9776.
(38) Yuan, B. L.; Pham, M.; Nguyen, T. H. Deposition kinetics of bacteriophage MS2 on a silica surface coated with natural organic matter in a radial stagnation point flow cell. *Environ. Sci. Technol.* **2008**, *42* (20), 7628−7633.
(39) da Silva, A. K.; Kavanagh, O. V.; Estes, M. K.; Elimelech, M. Adsorption and aggregation properties of norovirus GI and GII virus-like particles demonstrate differing responses to solution chemistry. *Environ. Sci. Technol.* **2011**, *45* (2), 520−526.
(40) Elimelech, M. Indirect evidence for hydration forces in the deposition of polystyrene latex colloids on glass surfaces. *J. Chem. Soc., Faraday Trans.* **1990**, *86* (9), 1623−1624.
(41) Verwey, E. J. W. Theory of the stability of lyophobic colloids. *Philips Res. Rep.* **1945**, *1* (1), 33−49.
(42) Derjaguin, B.; Landau, L. Theory of stability of highly charged liophobic sols and adhesion of highly charged particles in solutions of electrolytes. *Zh. Eksp. Teor. Fiz.* **1945**, *15* (11), 663−682.
(43) Franchi, A.; O'Melia, C. R. Effects of natural organic matter and solution chemistry on the deposition and reentrainment of colloids in porous media. *Environ. Sci. Technol.* **2003**, *37* (6), 1122−1129.
(44) Pelley, A. J.; Tufenkji, N. Effect of particle size and natural organic matter on the migration of nano- and microscale latex particles in saturated porous media. *J. Colloid Interface Sci.* **2008**, *321* (1), 74−83.
(45) Phenrat, T.; Song, J. E.; Cisneros, C. M.; Schoenfelder, D. P.; Tilton, R. D.; Lowry, G. V. Estimating attachment of nano- and submicrometer-particles coated with organic macromolecules in porous media: development of an empirical model. *Environ. Sci. Technol.* **2010**, *44* (12), 4531−4538.
(46) Thio, B. J. R.; Zhou, D. X.; Keller, A. A. Influence of natural organic matter on the aggregation and deposition of titanium dioxide nanoparticles. *J. Hazard. Mater.* **2011**, *189* (1−2), 556−563.
(47) Jaisi, D. P.; Saleh, N. B.; Blake, R. E.; Elimelech, M. Transport of single-walled carbon nanotubes in porous media: filtration mechanisms and reversibility. *Environ. Sci. Technol.* **2008**, *42* (22), 8317−8323.
(48) Beckett, R.; Jue, Z.; Giddings, J. C. Determination of molecular-weight distributions of fulvic and humic acids using flow field-flow fractionation. *Environ. Sci. Technol.* **1987**, *21* (3), 289−295.
(49) Shinozuka, T.; Shibata, M.; Yamaguchi, T. Molecular weight characterization of humic substances by MALDI-TOF-MS. *J. Mass Spectrom. Soc. Jpn.* **2004**, *52* (1), 29−32.
(50) Jiang, X. J.; Tong, M. P.; Li, H. Y.; Yang, K. Deposition kinetics of zinc oxide nanoparticles on natural organic matter coated silica surfaces. *J. Colloid Interface Sci.* **2010**, *350* (2), 427−434.
(51) de Kerchove, A. J.; Elimelech, M. Impact of alginate conditioning film on deposition kinetics of motile and nonmotile *Pseudomonas aeruginosa* strains. *Appl. Environ. Microbiol.* **2007**, *73* (16), 5227−5234.
(52) Hong, S. K.; Elimelech, M. Chemical and physical aspects of natural organic matter (NOM) fouling of nanofiltration membranes. *J. Membr. Sci.* **1997**, *132* (2), 159−181.